AIAA JOURNAL
Vol. 37, No. 12, December 1999

Thermal Effects on Chaotic Vibrations of Plates

Müge Fermen-Coker* and Glen E. Johnson†
University of Dayton, Dayton, Ohio 45469-0210

In recent years the investigation of dynamical behavior of plates under thermal loads has become important because of the high temperatures reached on external skin panels of hypersonic vehicles. Other researchers have indicated that the skin panels may encounter chaotic vibrations about their thermally buckled positions. In this research the chaotic vibrations of simply supported plates under thermal and sinusoidal excitation is studied to determine the predictability of the vibratory behavior of a representative class of such skin panels. The boundaries of regular and chaotic regions of motion are defined in force-temperature and force-frequency planes and the sensitivity of these boundaries to changes in design parameters is explored for the purpose of developing useful design criteria. The onset of chaos is predicted through the computation of Lyapunov exponents. The effects of thermal moment and thermal buckling on chaos are studied. The results of the research are presented as a contribution to the panel design of hypersonic vehicles.

Nomenclature

a = x dimension of rectangular plate
b = y dimension of rectangular plate
C_1 = coefficient of damping term in single-mode equation of motion
C_2 = coefficient of linear stiffness term in single-mode equation of motion
C_3 = coefficient of cubic stiffness term in single-mode equation of motion
C_4 = coefficient of forcing function in single-mode equation of motion
C_5 = coefficient of thermal gradient term in single-mode equation of motion
E = Young's modulus for plate material
F_{tg} = generalized thermal gradient forcing
F_0 = generalized excitation amplitude
h = plate thickness
K_c = generalized thermal coefficient for nonuniform temperature increase
K_u = generalized thermal coefficient for thermal gradient
K_0 = generalized thermal coefficient for constant temperature increase
K_1 = generalized linear stiffness
K_3 = generalized cubic stiffness
p_i = generalized mode for x displacement; for single mode, $i = 1$
q_i = generalized mode for y displacement; for single mode, $i = 1$
r_i = generalized mode for z displacement; for single mode, $i = 1$
U_B = bending component of strain energy
U_{int} = internal strain energy
U_S = strain energy caused by stretching of midplane
u = x displacement of midplane of plate; function of (x, y, t)
u_1 = assumed mode for u displacement
v = y displacement of midplane of plate; function of (x, y, t)
v_1 = assumed mode for v displacement
w = z displacement of midplane; function of (x, y, t)
w_1 = assumed mode for w displacement
x = direction parallel to edge of plate at midplane
y = direction parallel to edge of plate at midplane perpendicular to x
z = direction normal to midplane of plate perpendicular to x and y
α = coefficient of thermal expansion
β = generalized thermal buckling parameter
δ_0 = generalized modal deflection used as measure of forcing level
ζ = damping ratio
θ = temperature field; function of (x, y, z)
θ_u = constant temperature at $z = +h/2$ surface caused by thermal gradient, which is linear through the thickness of the plate
θ_0 = constant midplane temperature increase compared to a reference temperature state
$\theta_{0\text{cr}}$ = value of θ_0 that when acting alone causes buckling
ν = Poisson's ratio for plate material
τ = nondimensional time, t/t_n, where $t_n = 2\pi/\omega_n$
ω = forcing frequency
ω_n = lowest natural frequency of simply supported rectangular plate

Superscript

$(\,)'$ = derivative with respect to τ

Introduction

THE response of dynamical systems with two stable equilibrium states, such as vibrations of certain buckled structures, is studied frequently in the emerging field of chaotic dynamics, mainly to develop an intuitive understanding of how chaotic motions occur in a system. To constitute a model for such problems, Holmes[1] analyzed a simple nonlinear oscillator represented by Duffing's equation with negative linear stiffness. Dowell and Pezeshki[2] extended the work of Holmes by studying dynamics of a buckled beam. Their objective was to provide an improved understanding of why the chaotic oscillations occur and to compare their theoretical results with the experimental data provided by Moon.[3] Along the same research interests, Souza and Mook[4] studied the postbuckling dynamic response of an initially imperfect rigid-bar model with a linear rotational spring to a simple harmonic excitation, which is an important example of the similar structural systems that exhibit stable postbuckling behavior such as columns, beam columns, and plates.

Chaotic oscillations have been observed prior to the aforementioned studies. Kobayashi[5] and Dowell,[6] for example, reported observing irregular vibrations, in the 1960s. In 1971 Eastep and McIntosh[7] analyzed nonlinear flutter and response of a thin, elastic, simply supported plate and studied the stability of small perturbations about limit-cycle oscillation. They noted the nonlinear behavior of the interaction of the buckling and flutter phenomena but did

Received 1 May 1998; revision received 26 February 1999; accepted for publication 27 February 1999.

*Graduate Student, Department of Mechanical and Aerospace Engineering; currently Aerospace Engineer, Science Applications International Corporation, Lexington Park, MD 20634. Member AIAA.

†Professor and Chair, Department of Mechanical and Aerospace Engineering.

not specifically study it. In the 1980s, Dowell[8] considered the chaotic region in his discussion of the classical flutter-buckling stability diagram when he reanalyzed the flutter of a buckled plate. More recently, Galasyn[9] reported observing chaotic behavior in vibrating airframes. Some other recent studies include Refs. 10–13.

In this research the conditions under which simply supported plates subject to thermal and mechanical loading exhibit chaotic behavior are studied to develop a better understanding of the effects of operating conditions on the vibratory response of skin panels on vehicles that are subject to high-speed, high-temperature flight conditions. For the heated-plate problem studied here, the two-well potential form just discussed corresponds to the case where the uniform temperature at the midplate reaches a critical value, so that the negative thermal stiffness overcomes the linear part of the structural stiffness of the plate and the coefficient of the linear stiffness term becomes negative, which corresponds to the thermal buckling of the plate. The differences between the nature of the effects of thermal buckling and thermal moment on the vibrations of plates are investigated. Research in this area promises to explain important concepts such as acoustic fatigue, an important fluid-structure interaction problem, as the skin panels encounter chaotic vibrations about their thermally buckled positions.[14]

Equations of Motion

The equations of motion for the investigation of the large deflection of elastic plates subject to thermal and mechanical or aerodynamic loading may be developed in accordance with Ref. 15, employing an assumed mode method. As discussed in detail in Ref. 16, the development starts with Hamilton's extended principle. The linear stress-strain and strain-displacement relations are substituted into the strain-energy expression for the system, and von Kármán's large deflection theory and the Kirchhoff hypothesis are employed to obtain the strain energy of the heated plate in terms of the displacements u, v, and w. The strain energy has stretching and bending components:

$$U_{\text{int}} = U_S + U_B \tag{1}$$

where

$$\begin{aligned} U_S = {} & \iint \frac{Eh}{2(1-\nu^2)}\left(u_{,x} + \frac{1}{2}w_{,x}^2\right)^2 \mathrm{d}x\,\mathrm{d}y \\ & + \iint \frac{Eh}{2(1-\nu^2)}\left(v_{,y} + \frac{1}{2}w_{,y}^2\right)^2 \mathrm{d}x\,\mathrm{d}y \\ & + \iint \frac{Eh\nu}{(1-\nu^2)}\left(u_{,x} + \frac{1}{2}w_{,x}^2\right)\left(v_{,y} + \frac{1}{2}w_{,y}^2\right)\mathrm{d}x\,\mathrm{d}y \\ & + \iint \frac{Eh}{4(1+\nu)}(u_{,y} + v_{,x} + w_{,x}w_{,y})^2\,\mathrm{d}x\,\mathrm{d}y \\ & - \iint \frac{N_\theta}{(1-\nu)}\left(u_{,x} + v_{,y} + \frac{1}{2}w_{,x}^2 + \frac{1}{2}w_{,y}^2\right)\mathrm{d}x\,\mathrm{d}y \end{aligned} \tag{2}$$

$$\begin{aligned} U_B = {} & \iint \frac{D}{2}\left(w_{,xx}^2 + w_{,yy}^2\right)\mathrm{d}x\,\mathrm{d}y + \iint D\nu w_{,xx}w_{,yy}\,\mathrm{d}x\,\mathrm{d}y \\ & + \iint D(1-\nu)w_{,xy}^2\,\mathrm{d}x\,\mathrm{d}y + \iint \frac{M_\theta}{(1-\nu)}(w_{,xx} + w_{,yy})\,\mathrm{d}x\,\mathrm{d}y \end{aligned} \tag{3}$$

The simply supported boundary conditions are imposed on the system. Assuming only a single mode of vibration, the displacements are expanded as follows:

$$\begin{aligned} u &= hu_1(x, y)p_1(t) \\ v &= hv_1(x, y)q_1(t) \\ w &= hw_1(x, y)r_1(t) \end{aligned} \tag{4}$$

where the modal shape functions that satisfy the geometric boundary conditions are

$$u_1 = v_1 = w_1 = \sin\left(\frac{\pi x}{a}\right)\sin\left(\frac{\pi y}{b}\right) \tag{5}$$

Lagrange's equations of motion are[15,16]

$$\frac{\partial U_S}{\partial p_i} = 0 \tag{6}$$

$$\frac{\partial U_S}{\partial q_i} = 0 \tag{7}$$

$$\frac{\mathrm{d}}{\mathrm{d}t}\left(\frac{\partial T}{\partial_{\dot{r}_i}}\right) + \frac{\partial U_B}{\partial_{r_i}} + \frac{\partial U_S}{\partial_{r_i}} = Q_i \tag{8}$$

Note that, for the single-mode case, $i = 1$ in Eqs. (6–8). Evaluation of Lagrange's equations is quite complex and requires extensive algebraic manipulations because the integrals in the strain-energy expressions are carried out analytically, as opposed to the numerical evaluation of integrals in previous studies.[13,15] A symbolic mathematics program, Derive, is used for this purpose. Once this evaluation is accomplished, Eqs. (6) and (7) can be expressed in the following form:

$$\begin{bmatrix} [\boldsymbol{A}_1] & [\boldsymbol{B}_1] \\ [\boldsymbol{A}_2] & [\boldsymbol{B}_2] \end{bmatrix} \begin{Bmatrix} \{\boldsymbol{p}\} \\ \{\boldsymbol{q}\} \end{Bmatrix} = \begin{Bmatrix} \{\boldsymbol{C}_1(\{\boldsymbol{r}\})\} + \{\boldsymbol{d}_1(N_\theta)\} \\ \{\boldsymbol{C}_2(\{\boldsymbol{r}\})\} + \{\boldsymbol{d}_2(N_\theta)\} \end{Bmatrix} \tag{9}$$

Equations (9) may be solved for p_i and q_i in terms of r_i and can be substituted into Lagrange's third equation, Eq. (8).

For the single-mode case Lagrange's first equation, Eq. (6), becomes

$$\frac{\partial U_S}{\partial p_1} = \frac{3\pi^2[a^2(1-\nu) + 2b^2]}{2ab}p_1 = 0 \tag{10}$$

which implies that either $[a^2(1-\nu) + 2b^2] = 0$ or $p_1 = 0$. Because the former is impossible, the latter, i.e., $p_1 = 0$, must be true. Similarly, Lagrange's second equation, Eq. (7), reduces to

$$\frac{\partial U_S}{\partial q_1} = \frac{3\pi^2[b^2(1-\nu) + 2a^2]}{2ab}q_1 = 0 \tag{11}$$

indicating that $q_1 = 0$ must be true. Therefore, Lagrange's first two equations do not have any significance for the single-mode case, and the third equation is the only equation we need to consider. Equations of motion were also obtained considering four modes but with much difficulty because the software's capabilities were exceeded at times and hand manipulations were necessary. The resulting four coupled equations are listed in Ref. 16.

The thermal loading assumed includes a uniform temperature increase at the midplate, a parabolic temperature variation over the plate, and also a temperature gradient across the thickness of the plate to study the effects of global and local expansions that induce thermal buckling and the effects of thermal moments, respectively:

$$\theta(x, y, z) = \theta_0 + 16(x/a)(1 - x/a)(y/b)(1 - y/b)\theta_c + (2z/h)\theta_u \tag{12}$$

Once damping and sinusoidal external excitation are added to the system, Lagrange's equations of motion may be reduced as described in Ref. 16 to the single-mode equation of motion in nondimensional form:

$$r_1'' + C_1 r_1' + C_2 r_1 + C_3 r_1^3 = C_4 \sin(\Omega\tau) + C_5 \tag{13}$$

where

$$\begin{aligned} &C_1 = 4\pi\zeta, \qquad C_2 = 4\pi^2(1 - \beta_1), \qquad C_3 = 4\pi^2\frac{K_3}{K_1} \\ &C_4 = 4\pi^2\delta_0, \qquad C_5 = 4\pi^2 F_{\text{tg}}, \qquad \Omega = 2\pi\frac{\omega}{\omega_n} \\ &\beta_1 = C_{\theta_0}\theta_0 + C_{\theta_c}\theta_c, \qquad C_{\theta_0} = \frac{K_0}{K_1}, \qquad C_{\theta_c} = \frac{K_c}{K_1} \\ &K_1 = \frac{Eh^5\pi^4(a^2 + b^2)^2}{48a^3b^3(1-\nu^2)}, \qquad K_3 = \frac{Eh^5\pi^4(9a^4 + 2a^2b^2 + 9b^4)}{128a^3b^3(1-\nu^2)} \end{aligned} \tag{14}$$

$$K_0 = \frac{Eh^3\pi^2(a^2+b^2)}{4ab(1-\nu)}\alpha, \qquad K_c = \frac{Eh^3(a^2+b^2)(\pi^4-9)}{9ab\pi^2(1-\nu)}\alpha$$

$$\delta_0 = \frac{F_0}{K_1}, \qquad F_{\text{tg}} = \frac{16(1+\nu)\alpha}{\pi^4(h/a)^2}\theta_u$$

Note that the effects of both the uniform temperature term and the parabolic temperature variation term are incorporated in a single parameter β_1. When $\beta_1 > 1$, the linear stiffness term becomes negative, and this corresponds to buckling temperatures for the plate. The single-mode equation of motion, Eq. (13) just presented, is in the form of the well-known Duffing equation, which may be solved numerically to study the response of the system, using a simple computer code utilizing a fourth order Runge–Kutta integration scheme once the design variables are specified.

Numerical Approach

In this research, chaos is detected through the computation of Lyapunov exponents. Generally speaking, Lyapunov exponents provide a measure of the sensitive dependence of dynamical systems on initial conditions, which is one of the most important characteristics of chaotic behavior. The computation of Lyapunov exponents from a given set of differential equations is discussed in several books and papers such as Refs. 17–21, and it is demonstrated to be an effective tool to characterize chaotic motions by many researchers. One such study is performed by Pezeshki and Dowell,[22] who calculated the exponents for one-, two-, and four-mode modal projections of the partial differential equation governing the motion of a magnetically buckled beam. They successfully compared their numerically generated computations based on a technique presented in Ref. 18, which will also be employed here, to the exponents calculated from an experimental time history.

The single-mode, heated-plate equation (13) may easily be transformed into a set of three autonomous first order differential equations. Hence, the complete Lyapunov spectrum for this system consists of three Lyapunov exponents. Only the largest Lyapunov exponent needs to be computed for the purposes of this study, and this is done by employing a standard procedure discussed in references such as.[17–21] If the largest Lyapunov exponent is negative, it corresponds to a limit-cycle motion; if it is zero, it corresponds to two-torus; and if it is positive, it indicates a strange attractor, which, in turn, implies chaos.[17–21]

Note that the coefficients of the single-mode plate model given by Eq. (13) are not as well scaled as the coefficients of most Duffing equations previously studied in the literature. This difference seems to introduce some difficulties that require additional consideration regarding the practical computation of the Lyapunov exponents for the system. The convergence rate, in addition to being much slower in our case, is observed to be more sensitive to the choice of numerical scheme and the integration time step as well. When the largest Lyapunov exponent is calculated for a well-scaled set of coefficients that results in periodic motion, a fourth-order Runge–Kutta scheme and a higher-order method developed by Butcher, which is discussed in Refs. 23 and 24, are observed to produce identical solution curves. For a well-scaled set of coefficients again that produces chaotic motion, the solution curves obtained by using these two methods are found to be slightly different yet decidedly converging to a positive value as expected. On the other hand, when realistic values are specified as heated-plate problem parameters and are substituted into Eq. (13), the differences in the paths to the solution, obtained using various numerical integration schemes, may prove to be crucial, especially if a sufficient amount of time is not allowed for convergence. For the sake of comparison, the largest Lyapunov exponent estimates are obtained by employing three different methods. Because of the differences observed between the fourth-order Runge–Kutta solutions and the Butcher's method solutions, an International Mathematical and Statistical Libraries (IMSL) routine that utilizes a fifth- and sixth-order Runge–Kutta method is also used for verification. The differences in paths to the solution are observed to be misleading on occasion, even when the motion is not chaotic, as opposed to the case of well-scaled coefficients. Based on an extensive amount of numerical experiments, the utilization of Butcher's method is observed to result in a much better convergence rate and to give more reliable results compared to the other two methods in terms of providing a good comparison with the phase planes generated. Hence, Butcher's method is adapted to perform all of the Lyapunov exponent computations during the course of this study. Phase planes are generated using a standard fourth-order Runge–Kutta scheme for several points picked randomly to verify the Lyapunov exponent estimates.

A convergence criterion, based on various numerical experiments with our specific system, is developed, tested, and incorporated into the computer code that is used to compute the largest Lyapunov exponents, so that the procedure is automated. The main idea is to take averages of the oscillating values of the exponent estimates at regular intervals once the transients are discarded and to compare the resulting average value to the value already obtained each time, until the difference is smaller than a preset tolerance value. Hence, convergence of each exponent is checked automatically without having to examine the exponent estimates for each set of design variables studied.

The computational work presented here has been performed on Ohio Supercomputer Center's Cray Y-MP8E machine. Machine dependency was tested by running some of the cases on the Center's SGI Power Challenge System, using assisted parallelism. Effects of computational precision, i.e., 128-bit precision as opposed to 64-bit precision, and effects of different optimization levels were also investigated. The differences in results were insignificant, the comparison was generally good, and 64-bit precision is proven to be appropriate and sufficient for the purposes of this study. However, there seem to be certain regions in the design space where the motion is extremely sensitive to the slightest changes in parameters. For these values of the parameters, the machine round-off errors might lead to some inconsistencies between the results. For example, the machine representation of the number 1.67 when the loop is started with a smaller number and incremented to 1.67 might be 1.669999...5, and the machine representation of the number 1.67 when the loop is directly started with 1.67 might be 1.670000...2. In some cases even changes this small and seemingly insignificant may result in drastic changes in the predicted system behavior, and the system may behave chaotically for one case and periodically for the other. Therefore, one must take caution and be aware of this possibility when evaluating the results.

Thermal Buckling

Analytical Results

The modal potential energy of the system represented by Eq. (13) is

$$U_{r_1} = \tfrac{1}{4}C_3 r_1^4 + \tfrac{1}{2}C_2 r_1^2 - C_5 r_1 \tag{15}$$

which is obtained by realizing that the sum of all of the terms other than damping, excitation, and acceleration must be equal to the derivative of the potential energy with respect to the generalized mode for z displacement so that Lagrange's equation is satisfied. For simplicity, let us set $C_5 = 0$ for the time being, i.e., there is no difference between the temperatures of the upper and lower surfaces of the plate ($\theta_u = 0$). By setting the derivative of the potential energy expression with respect to r_1 to zero and substituting the original expressions stated in Eq. (14) for the coefficients, we obtain the equilibrium points as

$$r_1 = 0, \qquad r_1 = \pm\frac{2\sqrt{2}\sqrt{a^2+b^2}\sqrt{4a^2b^2\alpha(1+\nu)\left[\pi^4(9\theta_0+4\theta_c)-36\theta_c\right]-3\pi^6h^2(a^2+b^2)}}{3\pi^3|h|\sqrt{9a^4+2a^2b^2+9b^4}} \tag{16}$$

The critical value of uniform temperature increment after which linear stiffness becomes negative is the same value after which the term in the preceding square root becomes positive, and therefore the second and the third equilibrium points become real, constructing the twin-well potential form. In terms of the plate material and geometrical properties, this value is simply

$$\theta_{0\mathrm{cr}} = \frac{\pi^2 h^2 (a^2 + b^2)}{12 a^2 b^2 \alpha (1+\nu)} + 4\theta_c \left(\frac{1}{\pi^4} - \frac{1}{9} \right) \tag{17}$$

The coefficient of θ_c is roughly -0.4. For values of θ_0 greater than what is given by the preceding expression, the first equilibrium point at $r_1 = 0$ is an unstable equilibrium point, and the other two points in Eq. (16) are stable equilibrium points. As the amplitude of the forcing function is increased infinitesimally, the unstable equilibrium point evolves into an unstable saddle, and the two stable equilibrium points become stable period one attractors. When the amplitude is increased further, it is possible that either symmetric single-well attractors or cross-well attractors[25] occur.

At this point, we could make a couple of simple but important observations about the dependency of buckling temperatures on plate dimensions and material properties, just by examining Eq. (17). For materials with higher thermal expansion coefficient α or higher Poisson's ratio ν, less uniform temperature increase is needed for thermal buckling to occur. Young's modulus does not have any effect on this critical value; the thicker the plate, the later the buckling will occur as the temperature is increased. The closer the plate shape is to a square, the higher the temperatures that are needed to buckle the plate. For square plates, the bigger the dimensions of the plate are, the lower the critical uniform temperature is at the midplate that would buckle the plate.

Consider an aluminum plate of dimensions $a = 12$ in. (30.48 cm), $b = 50$ in. (127 cm), and $h = 0.2$ in. (0.508 cm). Let the damping coefficient be $\zeta = 0.01$. These values are substituted into Eq. (16), and θ_c is set equal to zero because the effect of both θ_0 and θ_c are essentially the same. There are three possibilities: 1) $\theta_0 > 13.94°\mathrm{F}$ ($\theta_0 > 7.74$ K), and there are three equilibrium points, which gives us the twin-well potential form; 2) $\theta_0 = \theta_{0\mathrm{cr}} = 13.94°\mathrm{F}$ ($\theta_0 = \theta_{0\mathrm{cr}} = 7.74$ K compared to a reference temperature state), which is the critical thermal buckling uniform temperature increment when θ_c and θ_u are set to zero, and the only equilibrium point is at $r_1 = 0$ in this case; and 3) $\theta_0 < 13.94°\mathrm{F}$ ($\theta_0 < 7.74$ K), and the only real root is at $r_1 = 0$. These results are demonstrated in Fig. 1, where the potential energy is shown as a function of θ_0 and r_1. It is clear how the potential energy transforms from single well to double well, making chaos possible. However, this outcome does not mean that after this critical value is reached that the dynamics of the system is mostly chaotic, as will be demonstrated later in the next section through the Lyapunov exponent computations.

Numerical Results

We calculated the value of θ_0 that would cause thermal buckling to be 13.94°F (7.74 K), when the plate parameters are specified as just stated. We may now employ the approach discussed in the Numerical Approach section of this paper and calculate the Lyapunov exponents for this plate. As discussed earlier, previous research in this area indicates that the sign of the coefficient of the linear stiffness term and the amplitude of the forcing function play crucial roles on the onset of chaos. Therefore, this will constitute our starting point. The dimensions, material properties, and damping are already fixed. Let us fix the frequency of external sinusoidal excitation at half the natural frequency and investigate the isolated combined effect of the excitation amplitude and uniform thermal loads at the midplate together. First, F_0 is varied between 10 and 1500 lb/in. in increments of 10 (between 1.13 and 169.48 Nm in increments of 1.13), and θ_0 is varied between 0 and 50°F in increments of 1 (between 0 and 27.78 K in increments of 0.56). The resulting curious pattern that exhibits the delicate nature of parametric sensitivity is displayed in Fig. 2. The blue tones represent the negative values of the largest Lyapunov exponent for each point and therefore define the regions of nonchaotic motion. The positive exponents, or the chaotic regions of motion, are represented with yellow and red tones. The white regions correspond to the points for which the calculated largest exponent is nearly zero.

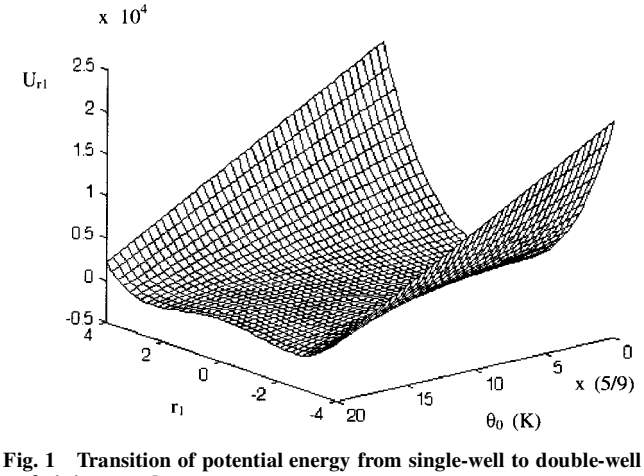

Fig. 1 Transition of potential energy from single-well to double-well as θ_0 is increased.

Phase portraits were generated to verify the results of the Lyapunov exponent computations displayed in Fig. 2. Even though the comparison was not favorable for some points corresponding to high-excitation amplitudes, the θ_0 range between 0 and 27.78 K and F_0 range between 1.13 and 22.6 Nm was relatively trouble free because our convergence criterion was satisfied at all of the data points; smaller step sizes were not needed during integration, and phase planes generated agreed with the results of the Lyapunov exponent computation. Therefore, we zoom into a smaller region and vary F_0 between 0.11 and 11.3 Nm in increments of 0.11 and θ_0 between 0 and 27.78 K in increments of 0.56. The result is shown in Fig. 3, representing 51×100 largest Lyapunov exponents. Notice that there is a highly chaotic region of motion around $\theta_0 = 48°\mathrm{F}$ ($\theta_0 = 26.67$ K) for very small amplitudes of excitation. There are a few points in Fig. 3, where the convergence criterion is not satisfied because the step sizes are now refined. The majority of these points are located around chaotic regions of motion, as one might expect, and the values of the calculated largest exponents are relatively close to zero.

If we zoom once again into a smaller region where F_0 is now varied between 0.5 and 3.5 lb/in. by 0.1 (between 0.0565 and 0.395 Nm by 0.011), and θ_0 is varied between 13 and 18°F (between 7.22 and 10 K), as shown in Fig. 4, we magnify a small chaotic region that represents the first onset of chaos for this specific aluminum plate with the given dimensions. The results are verified through examining the phase portraits. We should note that smaller time steps were not needed for any of the points in this region. However, there are some points around the boundaries of the chaotic region where the convergence criterion is not satisfied.

The sharp edge on the left side of the chaotic region shown in Fig. 4 simply means that for F_0 between 1.5 and 3 lb/in. (between 0.17 and 0.34 Nm) the critical temperature for the onset of chaos is constant at approximately 14.4°F (8 K). We observe the same curious pattern of sharp left edges of chaotic regions in Figs. 3 and 4.

The critical thermal buckling uniform temperature increment at the midplate was previously obtained for the plate we are studying to be 13.94°F (7.74 K). Figures 2–4 indicate that chaos occurs some time after this value is reached for relatively lower values of F_0, as expected. For example, for Fig. 4 there seems to be a very definite critical value for chaos at 14.4°F (8 K) for most of the amplitudes within this range. For each value of F_0, one may extract the corresponding critical values of θ_0 after which chaos is possible, or vice versa, by writing a simple computer code.

Note that an interesting transformation takes place as the amplitude of the external excitation reaches somewhere between 110 and 120 lb/in. (between 12.43 and 13.56 Nm). After this critical value of F_0, the values of $\theta_{0\mathrm{cr}}$ become less than the already determined analytical value of 13.94°F (7.74 K), indicating single-well chaos.

Even though globally we observe that lower temperatures are needed for chaos to occur as the amplitude gets higher, we cannot make a generalization because there is no direct proportionality by any means and locally the expectations could be quite different.

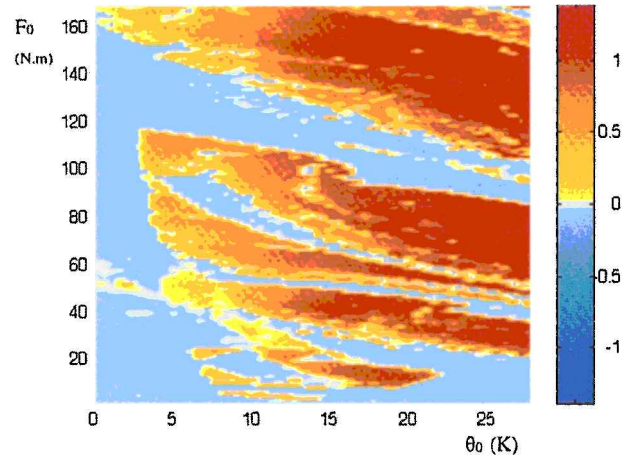

Fig. 2 Largest Lyapunov exponent depicted in color as a function of θ_0 and F_0 for $\theta_u = 0$.

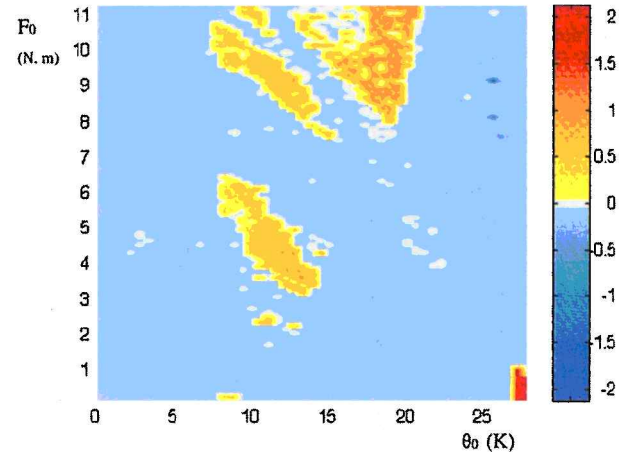

Fig. 3 Largest Lyapunov exponent depicted in color as a function of θ_0 and F_0 for $\theta_u = 0$.

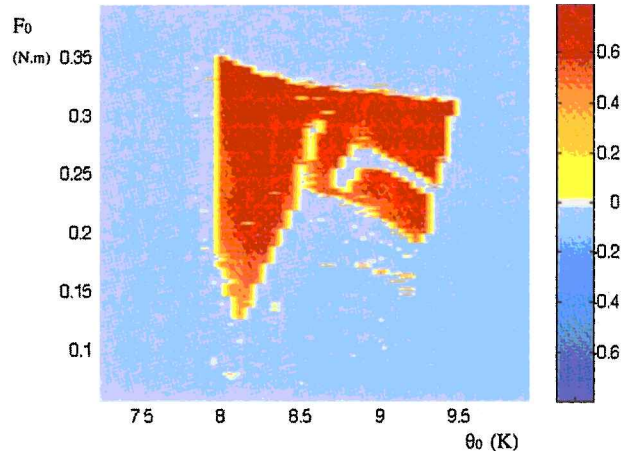

Fig. 4 Largest Lyapunov exponent depicted in color as a function of θ_0 and F_0 for $\theta_u = 0$.

For example, for F_0 equal to 1030 lb/in. (116.37 Nm), the critical value of θ_0 for chaos is 6°F (3.33 K), but for F_0 equal to 1040 lb/in. (117.5 Nm), the critical value of θ_0 for chaos is 32°F (17.78 K). Therefore, unless one has portraits of chaos as shown here, it is impossible to guess a critical θ_0 corresponding to a certain amplitude of excitation. As indicated by these results, at F_0 around 1500 lb/in. (169.48 Nm) no temperature increase is needed at all for the motion to be chaotic for the simply supported plate considered here.

These results indicate that one may determine certain intervals of the amplitude of excitation for which a critical midplate temperature for chaos is constant. Most importantly, one can also determine acceptable ranges of excitation amplitude for which chaos is very much delayed or maybe does not exist at all within the operating temperatures, as in the case of F_0 between 10 and 17 lb/in. (1.13 and 1.92 Nm), for example.

Note that the equation of motion, Eq. (13), is set up so that performing a similar analysis for the case of a plate with a hot center and relatively cooler sides, i.e., a parabolic temperature increase profile over the midsurface, is also possible. The effect of such a temperature distribution is expected to have the same fundamental effect as that of the uniform temperature increase. The hotter temperatures at the midplate are expected to simply shift the results obtained to the left, i.e., to lower temperatures. Therefore, the computations related to the parabolic temperature increase profile are not performed separately.

Thermal Moment

Analytical Results

A temperature difference is imposed between the upper and lower surfaces of the plate to investigate how the onset of chaos and the boundaries of the chaotic regions of motion are effected by this newly introduced thermal gradient across the thickness. Because the problem is symmetrical with respect to the middle surface of the plate, only the case of higher upper-surface temperatures than the lower-surface temperatures is considered, so that the plate is forced to bend concave up.

The critical temperature increase for chaos to occur is observed to be at 14.4°F (8 K) for the specific range of excitation amplitudes shown in Fig. 4, provided that the plate dimensions and material properties are as already stated. For temperatures slightly higher than this temperature, the motion is chaotic in a postbuckling state. $\theta_0 = 15$°F (8.33 K) is picked within this chaotic region, and the effect of increasing the thermal gradient across the plate's thickness is investigated.

The potential energy of the system is analyzed by cutting a slice of the potential energy function displayed in Fig. 1 at $\theta_0 = 15$°F (8.33 K), converting it to a two-dimensional form to observe the effect of increased thermal gradient better. The solid line constituting the double-well potential form shown in Fig. 5 displays the case where the thermal gradient is zero. The dashed and dotted lines demonstrate how the two-well form gradually transforms itself to favor a single-well form as the upper surface temperature is increased relative to the midsurface and lower-surface temperature. As the upper surface of the plate gets hotter compared to the lower surface of the plate the propensity of the plate to deform concave up is increased, which reduces the unpredictability of the state of bifurcation when the critical thermal buckling temperature is reached at the midsurface. This, in turn, reduces the possibility for chaos to occur.

The critical value of θ_u after which one of the wells disappears can be found by setting the derivative of U_{r_1} presented in Eq. (15) to zero. The resulting equation is a cubic equation, the solution of

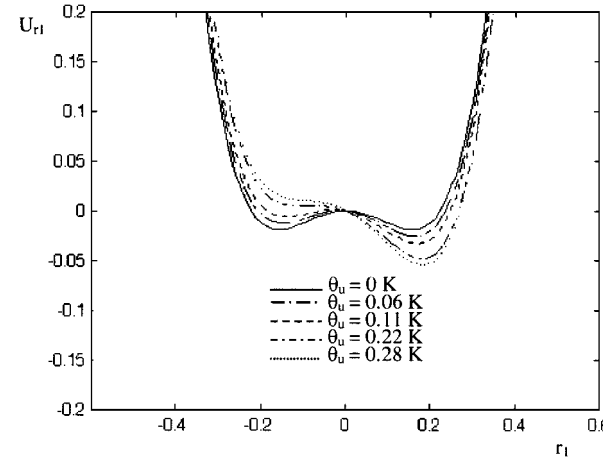

Fig. 5 Thermal gradient effect: r_1 vs U_{r_1} for various values of θ_u, where $\theta_0 = 8.33$ K.

which leads us to Eq. (18):

$$\theta_{u_{cr}} = \frac{\sqrt{2}\pi\sqrt{(a^2+b^2)}\sqrt{\left[12\alpha a^2b^2\theta_0(1+\nu)-\pi^2h^2(a^2+b^2)\right]^3}}{72a^2b^2|\alpha h(1+\nu)|\sqrt{9a^4+2a^2b^2+9b^4}} \tag{18}$$

Substituting the geometrical and material properties of the plate, as already stated, into this expression, and also setting $\theta_0 = 15°$F (8.33 K) as in our current example of Fig. 5, the critical upper-surface temperature increase is obtained to be 0.24°F (0.133 K). That is, a temperature difference of approximately half a degree Fahrenheit is needed between the upper and lower surfaces when the midsurface temperature is increased by 15°F (8.33 K), in order to eliminate the two-well potential form. We realize of course that this analysis is independent of the amplitude of the forcing function. The overall response of the system depends highly on the excitation amplitude as well as the thermal loads and the potential energy of the system.

Numerical Results

Let us now confirm our results by examining the motion in the region shown by Fig. 4 with the addition of a temperature differential across the thickness. This will also bring some insight into the combined effect of thermal gradient and external excitation amplitudes. We set $\theta_u = 0.5°$F (0.28 K) and recalculate the Lyapunov exponents in the region of Fig. 4. The result is shown in Fig. 6. The regions are considerably smaller, and for most amplitudes chaos is delayed significantly. Although unlikely to be achieved, $\theta_u = 1°$F (0.56 K) is forced this time, and this particular chaotic region in question is almost completely eliminated, as shown in Fig. 7. Note that the values of the Lyapunov exponents are significantly smaller in Fig. 7 than in Figs. 5 and 6.

A comparison between the critical lines of uniform temperature increase at the midplate for chaos to occur, for the zero gradient case

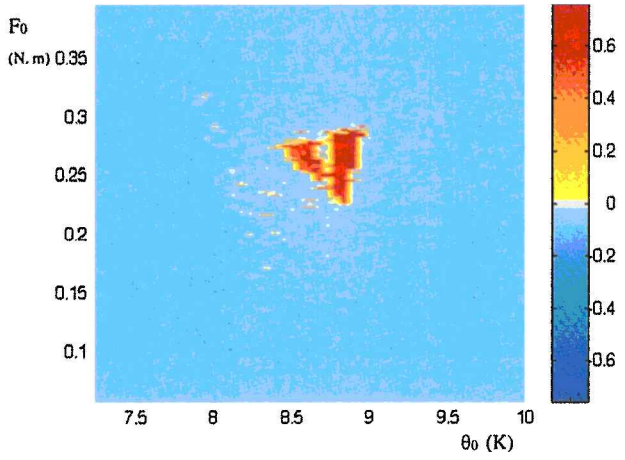

Fig. 6 Largest Lyapunov exponent depicted in color as a function of θ_0 and F_0 for $\theta_u = 0.28$ K.

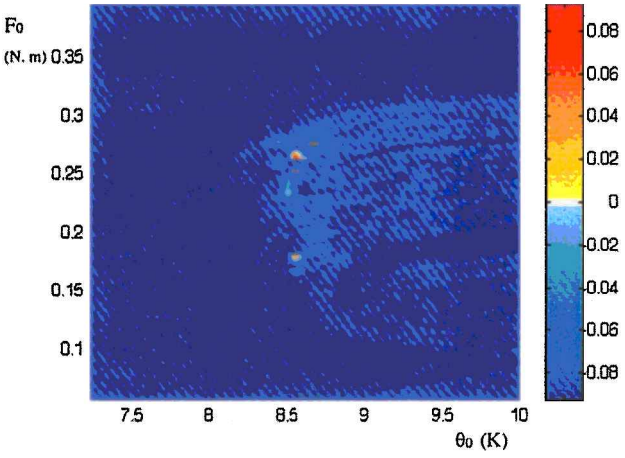

Fig. 7 Largest Lyapunov exponent depicted in color as a function of θ_0 and F_0 for $\theta_u = 0.56$ K.

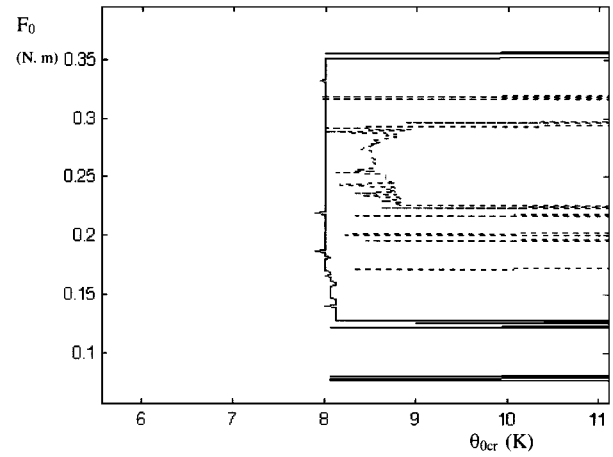

Fig. 8 Critical values of θ_0 vs F_0 for $\theta_u = 0$ and $\theta_u = 0.28$ K.

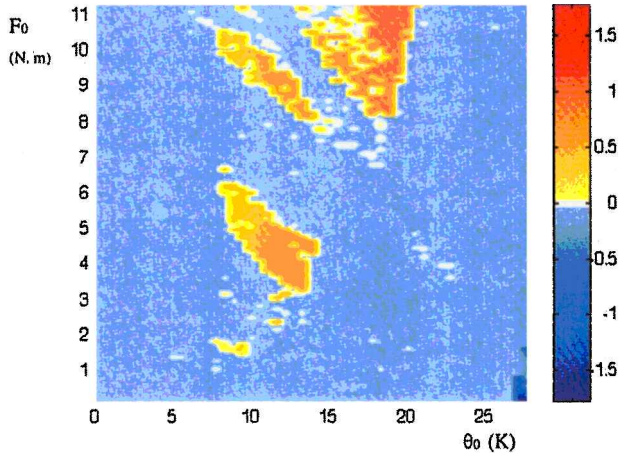

Fig. 9 Largest Lyapunov exponent depicted in color as a function of θ_0 and F_0 for $\theta_u = 0.28$ K.

of Fig. 4, and the $\theta_u = 0.5°$F (0.28 K) case of Fig. 6 is provided by Fig. 8. The critical values corresponding to the increased gradient case are clearly higher than the zero gradient case. Also, note that the vertical left edge of the critical θ_0 values shown next is delayed not by a constant factor to the right but rather eliminated completely. The region got smaller, and the shape changed.

The next logical step is to investigate how the amplitude of the forcing function effects the motion of the system, under the influence of thermal gradient, in addition to the temperature increase at the midplate. A larger region, which was presented in Fig. 3, originally was reexamined because it contains much larger amplitudes, and the largest Lyapunov exponents are calculated one more time for this region by setting $\theta_u = 0.5°$F (0.28 K). The result is shown in Fig. 9. The tiny region at the bottom of Fig. 9, which we had magnified to obtain Fig. 4 before, has disappeared, as our preceding results indicate. The bigger region at the right lower corner of the figure is no longer chaotic. The step sizes need to be refined to make conclusions that are more accurate. However, it is safe to conclude that, as the amplitude of the external excitation is increased, the influence of increased thermal gradient across the thickness becomes less and less significant. This makes sense physically because the thermal gradient increases the tendency of the plate to buckle in a certain direction as long as the amplitude of the excitation is not strong enough to compensate for this inclination. For smaller amplitudes, however, the effect of thermal gradient could be quite significant in terms of delaying or eliminating chaos.

Conclusions

The single-mode equation of motion suitable for the investigation of large deflection of elastic plates subject to mechanical and thermal loads is developed and presented so that the conditions under which plates, modeling skin panels on hypersonic, transatmospheric vehicles, exhibit chaotic behavior may be studied. The equations are

simplified by imposing simply supported boundary conditions and a sinusoidal external excitation. Thermal loads are assumed to include a uniform temperature increase at the midplate, a parabolic temperature variation over the plate, and also a temperature gradient across the thickness of the plate to study the effects of global and local expansions that induce thermal buckling and the effects of thermal moments, respectively. The single-mode equation obtained is employed to gain some preliminary insight into understanding the effects of changes in mechanical and thermal loading conditions on the chaotic behavior of the system.

The response of the system to uniform heating is considered. The critical value of the midplate temperature compared to a reference state, after which the linear stiffness term in the single-mode equation that is of Duffing form becomes negative, is obtained analytically in terms of the material and geometric properties of the plate, so that the two-well potential criterion may be applied. The largest Lyapunov exponent is calculated as the midplate temperature is varied as well as the forcing amplitude, and the results are displayed in force-temperature planes that display the combined effect of these two parameters on the chaotic response of the system. The first onset of chaos is detected in the force-temperature plane by specifying the material and geometric properties of the plate and is shown to cover a very narrow margin of amplitudes and temperatures. The qualitative pictures of the force-temperature planes indicate that the critical temperature for the onset of chaos is constant for certain ranges of amplitudes, sporadically. For the specified plate parameters the critical temperature for the onset of chaos is observed to be higher than the analytically determined critical buckling temperature, especially when the forcing amplitudes are relatively low. The critical temperatures for chaos are perceived to be inversely proportional to the excitation amplitudes, with the exception of chaos-free amplitudes.

For the whole range of midplate temperatures studied here, there exists an excitation amplitude for which the motion is chaotic and after which chaos is possible. However, there also exist a large number of chaos-free regions in the force-temperature planes generated. A critical value of excitation amplitude, after which chaos occurs prior to the analytically determined critical buckling temperature, is observed.

A linear temperature differential is introduced between the upper and lower surfaces of the panel to investigate the dynamical behavior of the system when a thermal moment is involved. An analytical expression for the critical value of the upper-surface temperature is obtained in terms of material and geometric properties of the plate. We demonstrated that the two-well potential form gradually transforms itself to favor a single-well form as the thermal moment is increased. This result is verified through the computation of Lyapunov exponents and is clearly demonstrated in the force-temperature planes generated throughout this research. The already detected chaotic regions are shown to get smaller in size, and chaos is delayed, or completely eliminated in some cases, as the thermal gradient is increased. However, this thermal moment effect is reduced gradually as the amplitude of excitation is increased.

Acknowledgments

The computational work presented here was performed on Ohio Supercomputer Center's Cray Y-MP8E machine. The authors wish to thank the Ohio Supercomputer Center personnel, especially Leslie Southern, Al Stutz, Larry Cooper, David Ennis, Tim Rozmajzl, and Armen Ezekielian, for their assistance and cooperation.

References

[1]Holmes, P. J., "A Nonlinear Oscillator with a Strange Attractor," *Philosophical Transactions of the Royal Society of London*, Vol. 292, No. 1394, 1979, pp. 419–448.

[2]Dowell, E. H., and Pezeshki, C., "On the Understanding of Chaos in Duffing's Equation Including a Comparison with Experiment," *Journal of Applied Mechanics*, Vol. 53, March 1986, pp. 5–9.

[3]Moon, F. C., "Experiments on Chaotic Motions of a Forced Nonlinear Oscillator: Strange Attractors," *Journal of Sound and Vibration*, Vol. 85, No. 3, 1982, pp. 333–344.

[4]Souza, M. A., and Mook, D. T., "Post-Buckling Nonlinear Vibrations of Initially Imperfect Structural Systems," *Proceedings of the AIAA/ASME/ASCE/AHS/ASC 32nd Structures, Structural Dynamics, and Materials Conference*, AIAA, Washington, DC, 1991, pp. 2772–2775.

[5]Kobayashi, S., "Two Dimensional Panel Flutter 1. Simply Supported Panel," *Transactions of the Japan Society for Aeronautical and Space Sciences*, Vol. 5, No. 8, 1962, pp. 90–102.

[6]Dowell, E. H., "Nonlinear Oscillations of a Fluttering Plate," *AIAA Journal*, Vol. 4, No. 7, 1966, pp. 1267–1275.

[7]Eastep, F. E., and McIntosh, S. C., Jr., "Analysis of Nonlinear Panel Flutter and Response Under Random Excitation or Nonlinear Aerodynamic Loading," *AIAA Journal*, Vol. 9, No. 3, 1971, pp. 411–418.

[8]Dowell, E. H., "Flutter of a Buckled Plate as an Example of Chaotic Motion of a Deterministic Autonomous System," *Journal of Sound and Vibration*, Vol. 85, No. 3, 1982, pp. 333–344.

[9]Galasyn, J., "Observation of Chaotic Dynamics in Vibrating Airframes," *Proceedings of the AIAA Fight Simulation Technologies Conference*, AIAA, Washington, DC, 1991, pp. 286–299.

[10]Murphy, K. D., Virgin, L. N., and Rizzi, S. A., "Characterizing the Dynamics Response of a Thermally Loaded Acoustically Excited Plate," *Journal of Sound and Vibration*, Vol. 196, No. 5, 1996, pp. 635–658.

[11]Murphy, K. D., Virgin, L. N., and Rizzi, S. A., "Experimental Snap-Through Boundaries for Acoustically Excited Thermally Buckled Plates," *Experimental Mechanics*, Vol. 36, No. 4, 1996, pp. 312–317.

[12]Hopkins, M. A., and Dowell, E. H., "Limited Amplitude Panel Flutter with a Temperature Differential," AIAA Paper 94-1486, April 1994.

[13]Hopkins, M. A., "Nonlinear Response of a Fluttering Plate Subject to Supersonic Aerodynamic, Thermal, and Pressure Loads," Ph.D. Dissertation, Dept. of Mechanical Engineering and Materials Science, Duke Univ., Durham, NC, 1994.

[14]Lee, J., "Large-Amplitude Plate Vibration in an Elevated Thermal Environment," *Applied Mechanics Reviews*, Vol. 46, No. 11, Pt. 2, 1993, pp. 242–254.

[15]Weiliang, Y., and Dowell, E. H., "Limit Cycle Oscillations of a Fluttering Cantilever Plate," *AIAA Journal*, Vol. 29, No. 11, 1991, pp. 1929–1936.

[16]Fermen-Coker, M., "Chaotic Vibrations of Heated Plates," Ph.D. Dissertation, Dept. of Mechanical and Aerospace Engineering, Univ. of Dayton, Dayton, OH, 1998.

[17]Schuster, H. G., *Deterministic Chaos: An Introduction*, VCH, Weinheim, Germany, 1989.

[18]Wolf, A., Swift, J. B., Swinney, H. L., and Vastano, J. A., "Determining Lyapunov Exponents from a Time Series," *Physica*, Vol. 16D, 1985, pp. 285–317.

[19]Benettin, G., Galgani, L., Giorgilli, A., and Strelcyn, J. M., "Lyapunov Characteristic Exponents for Smooth Dynamical Systems and for Hamiltonian Systems: A Method for Computing All of Them," *Meccanica*, Vol. 15, March 1980, pp. 21–30.

[20]Baker, G. L., and Gollub, J. P., *Chaotic Dynamics: An Introduction*, Cambridge Univ. Press, Cambridge, England, UK, 1990.

[21]Korsch, H. J., and Jodl, H.-J., *Chaos: A Program Collection for the PC*, Springer–Verlag, New York, 1994.

[22]Pezeshki, C., and Dowell, E. H., "Generation and Analysis of Lyapunov Exponents for the Buckled Beam," *International Journal of Non-Linear Mechanics*, Vol. 24, No. 2, 1989, pp. 79–97.

[23]James, M. L., Smith, G. M., and Wolford, J. C., *Applied Numerical Methods for Digital Computation*, Harper and Row, New York, 1993.

[24]Butcher, J. C., "On Runge-Kutta Processes of Higher Order," *Journal of Australian Mathematical Society*, Vol. 4, Pt. 2, 1964, pp. 179–194.

[25]Katz, A. L., and Dowell, E. H., "From Single Well Chaos to Cross Well Chaos: A Detailed Explanation in Terms of Manifold Intersections," *International Journal of Bifurcation and Chaos*, Vol. 4, No. 4, 1994, p. 993.

A. Berman
Associate Editor